Experimental and numerical characterisation of the cyclic thermo-mechanical behaviour of a high temperature forming tool alloy

EXPERIMENTAL AND NUMERICAL CHARACTERISATION OF THE CYCLIC THERMO-MECHANICAL BEHAVIOUR OF A HIGH TEMPERATURE FORMING TOOL ALLOY

Sean B Leen[1], Aditya Deshpande[2], Thomas H Hyde[2]

[1]Mechanical and Biomedical Engineering, College of Engineering and Informatics, NUI Galway, Galway, Ireland, sean.leen@nuigalway.ie; [2]Department of Mechanical, Materials & Manufacturing Engineering, Faculty of Engineering, University of Nottingham, UK, epxaad@nottingham.ac.uk; Thomas.hyde@nottingham.ac.uk

ABSTRACT

This paper describes high temperature cyclic and creep relaxation testing and modelling of a high nickel-chromium material (XN40F) for application to the life prediction of superplastic forming (SPF) tools. An experimental test programme to characterise the high temperature cyclic elastic-plastic-creep behaviour of the material over a range of temperatures between 20^{o}C and 900^{o}C is described. The objective of the material testing is the development of a high temperature material model for cyclic analyses and life prediction of superplastic forming (SPF) dies for SPF of titanium aerospace components. A two-layer visco-plasticity model which combines both creep and combined isotropic-kinematic plasticity is chosen to represent the material behaviour. The process of material constant identification for this model is presented and the predicted results are compared with the rate-dependent (isothermal) experimental results. The temperature-dependent material model is furthermore applied to simulative thermo-mechanical fatigue (TMF) tests, designed to represent the temperature and stress-strain cycling associated with the most damaging phase of

the die cycle. The model is shown to give good correlation with the test data, thus vindicating future application of the material model in thermo-mechanical analyses of SPF dies, for distortion and life prediction.

INTRODUCTION

Superplastic forming tools need to withstand high temperature cyclic loading and steady mechanical loading for extended durations and therefore are manufactured (by casting) from specialized alloys, but at the same time numerous additional geometrical complexities result from weight-saving constraints (due for example to weight limitations in industrial plant related to handling capacities) and ruling section requirements for casting. The cost of tool failure is significant and tool life is an important limiting aspect in the SPF process; the SPF process is a high value-added process, rather than a mass production process.

Large SPF tools mainly suffer from distortion due to thermal cycling and high temperature creep. Creep relaxation during forming induces inelastic deformation and distortion of the tool after cooling to the ambient [1]. Finite element (FE) based simulation of realistic thermo-mechanical conditions is an effective method for analysing realistic large SPF tool behaviour to predict the complex temperature-stress-strain cycles. However the choice of material behaviour models is important for FE-based life and performance (e.g. distortion) predictions.

A two-layer viscoplasticity material model is investigated here to analyse the thermo-mechanical behaviour of SPF tool made of 40% nickel and 20% chromium alloy (XN40F). The model combines the cyclic plasticity and creep via a partitioning of stress into elastic-viscous and elastic-plastic components in parallel with each other. The time-independent cyclic plasticity is modelled using the Chaboche combined

non-linear kinematic-isotropic hardening model and the time- dependent behaviour is captured using a power law creep model.

The cyclic plasticity material constitutive constants are identified from the tests across the range of relevant temperatures of 20^{o}C to 900^{o}C by varying the strain-ranges and the identification process is carried out for two different strain-rates, corresponding to predicted representative conditions for SPF dies. Power law creep constants for steady state secondary creep were identified from stress relaxation tests carried out at 500, 700 and 900˚C, although negligible creep occurred at 500˚C.

The material models and identified material constants are validated against the isothermal and thermo-mechanical fatigue and fatigue-creep tests.

MATERIAL TESTING

An Instron thermo-mechanical fatigue test rig is employed to carry out the high temperature material testing. The test machine uses a servo-electric dynamic loading system with induction coil heating to achieve the high temperatures required to simulate the die operating conditions. Figure 1 shows the fatigue specimen employed and the induction coil (at a temperature of 900°C) with the ceramic-rod extensometer in-situ to help effect strain control.

Temperature uniformity over the gauge length of ±10°C for 200°C to 900°C has been achieved using careful design of the induction coil and measurement using a number of contact thermocouples [2]. The specified heating and cooling rates of the test machine are 50±10 ^{o}C/sec and 25±10 ^{o}C/sec, respectively. Automated thermal strain compensation and Young's modulus determination to impose the target mechanical strain are implemented within the system according to the ASTM thermo-mechanical fatigue testing standard.

The SPF tool is cast from XN40F material (Aubert and Duval). The composition of XN40F tool material is given in Table 1 while the thermal properties are given in Table 2. Thermal properties such as thermal conductivity and specific heat at different temperatures are required to predict the thermal histories of the SPF tool.

Cyclic multiple strain range isothermal tests were carried out at temperatures of 20˚C, 500˚C, 700˚C and 900˚C for two strain rates, 5×10^{-3} s^{-1} and 5×10^{-4} s^{-1}, to characterise the temperature-dependent cyclic stress-strain behaviour of the XN40F alloy.

Lower strain-ranges were employed for the lower temperatures, consistent with anticipated relevant in-situ conditions. Table 4 summarises the complete test programme. Figure 2 shows the stabilized cyclic stress-strain curves obtained from the tests at different temperatures.

Figure 3 shows the evolution of the stress-strain loops at 20, 500, 700 and 900˚C for the first 30 or so cycles at a strain range of 0.6%. For the at 20˚C, 500˚C and 700˚C cases, cyclic hardening is observed with stabilization after 30 cycles. Negligible cyclic hardening was observed at 900˚C, i.e. stabilization occurs on the first cycle.

In addition to cyclic tests, isothermal stress relaxation tests were carried out at 500, 700 and 900˚C to identify secondary creep constants, via a strain-hold of 0.15% strain in tension. No stress relaxation was observed for the 500˚C test. Figure 4 shows the measured stress relaxation during the strain hold period of 360 seconds for 700 and 900ºC temperatures. At 900ºC, the stress relaxed from 83 MPa to 9 MPa whereas at 700ºC stress relaxation occurred from 155 MPa to 72 MPa.

MATERIAL BEHAVIOUR MODELLING

The two-layer viscoplastic model [4,5] was developed for modelling materials in which significant time dependent as well as time independent behaviour is observed which is generally the case for high temperature deformation. It is particularly intended for modelling material behaviour under loading fluctuations over a wide range of temperatures. Figure 5 shows a one dimensional rheological depiction of the model, which comprises an elastic–plastic network in parallel with an elastic–viscous (Maxwell model) network.

The elasto-plastic network predicts the time independent behaviour of the material whereas the elastic-viscous network predicts the time dependent behaviour of the material. In this model, the two mechanisms are assumed to be independent and therefore the total stress $\boldsymbol{\sigma}$ is decomposed into the stress $\boldsymbol{\sigma}_p$ in the elastic-plastic network and the stress $\boldsymbol{\sigma}_v$ in the elastic-viscous network.

In this paper, the two-layer model is temperature-dependent with a combined non-linear kinematic and isotropic hardening cyclic plasticity model for the time-independent behaviour and a Norton power law (secondary creep) behaviour for the (time-dependent) viscoplastic behaviour. The Ziegler kinematic hardening law [6] is used to simulate the translation of the yield surface in the stress space, through the back stress, $\boldsymbol{\alpha}$.

The multiaxial equations for the two-layer viscoplastic model are defined as follows:

$$\boldsymbol{\varepsilon}_v^{el} = \frac{1+\nu}{K_v}\boldsymbol{\sigma}_v - \frac{\nu}{K_v} tr(\boldsymbol{\sigma}_v)\boldsymbol{I} \tag{1}$$

$$\boldsymbol{\varepsilon}_p^{el} = \frac{1+\nu}{K_p}\boldsymbol{\sigma}_p - \frac{\nu}{K_p} tr(\boldsymbol{\sigma}_p)\boldsymbol{I} \tag{2}$$

$$\boldsymbol{\sigma}_v = \boldsymbol{K}_v : \left(\boldsymbol{\varepsilon} - \boldsymbol{\varepsilon}_v\right) \tag{3}$$

$$\boldsymbol{\sigma}_p = \boldsymbol{K}_p : \left(\boldsymbol{\varepsilon} - \boldsymbol{\varepsilon}_p\right) \tag{4}$$

$$\boldsymbol{\sigma} = \boldsymbol{\sigma}_p + \boldsymbol{\sigma}_v \tag{5}$$

with the yield surface defined by:

$$f\left(\boldsymbol{\sigma}_p - \boldsymbol{\alpha}\right) = \sigma^0 \tag{6}$$

where σ^0 is the current size of the yield surface and $f\left(\boldsymbol{\sigma}_p - \boldsymbol{\alpha}\right)$ is the equivalent (von Mises) stress with the back stress $\boldsymbol{\alpha}$ defined as:

$$f\left(\boldsymbol{\sigma}_p - \boldsymbol{\alpha}\right) = \sqrt{\frac{3}{2}\left(\boldsymbol{S}_p - \boldsymbol{\alpha}^{dev}\right) : \left(\boldsymbol{S}_p - \boldsymbol{\alpha}^{dev}\right)} \tag{7}$$

where $\boldsymbol{\alpha}^{dev}$ is the deviatoric part of the back stress and $\boldsymbol{S}_p$ is the deviatoric (plastic) stress tensor. The plastic flow-rule is:

$$\dot{\boldsymbol{\varepsilon}}_p = \frac{\partial f\left(\boldsymbol{\sigma}_p - \boldsymbol{\alpha}\right)}{\partial \boldsymbol{\sigma}_p} p \tag{8}$$

where p is the equivalent plastic strain rate defined as follows:

$$p = \sqrt{\frac{2}{3}\dot{\boldsymbol{\varepsilon}}_p : \dot{\boldsymbol{\varepsilon}}_p} \tag{9}$$

Cyclic hardening behaviour of the material is captured using an exponential law where the size of the yield surface σ^0 can be defined as a function of equivalent plastic strain, p, and temperature.

$$\sigma^0 = k + Q_\infty\left(1 - \exp(-bp)\right) \tag{10}$$

Here k is the size of the yield surface at zero plastic strain and Q_∞ and b are material constants to be identified from cyclic stress-strain loops.

The evolution of the kinematic hardening component is given below. The size of the yield surface is a function of temperature T and the generalised Ziegler's rule for the an-isothermal case is given as

$$\dot{\boldsymbol{\alpha}} = C\dot{p}\frac{1}{\sigma^0}\left(\boldsymbol{\sigma}_p - \boldsymbol{\alpha}\right) - \gamma\alpha\dot{p} + \frac{1}{C}\boldsymbol{\alpha}\dot{C} \tag{11}$$

where $C(T)$ is the temperature-dependent hardening modulus of the isothermal uni-axial stress-strain response, $\frac{\partial \boldsymbol{\sigma}}{\partial p}$, measured at different temperatures, $\dot{C}$ is the rate of change of C with respect to temperature and $\gamma\alpha\dot{p}$ is a recall term to introduce non-linearity in the evolution law.

The steady state (secondary) creep behaviour is modelled using the Norton power-law as follows:

$$\dot{\boldsymbol{\varepsilon}}_v = \frac{3}{2}A\left[f(\boldsymbol{\sigma}_v)\right]^n \frac{\boldsymbol{S}_v}{f(\boldsymbol{\sigma}_v)} \tag{12}$$

where A and n are temperature-dependent material constants, $\dot{\boldsymbol{\varepsilon}}_v$ is the viscous creep strain rate and $\boldsymbol{S}_v$ is the deviatoric viscous stress tensor.

As implemented in ABAQUS, a user-defined, temperature-dependent, parameter f is introduced to define the relative magnitudes of K_V, the elastic modulus of elastic-viscous network, and K_P+K_V, the total instantaneous elastic modulus (assumed to equal E, Young's modulus), as follows:

$$f = \frac{K_v}{K_v + K_p} \tag{13}$$

However the f value here is identified by fitting the two layer model with the stress relaxation test data using identified creep constants from the tests.

IDENTIFICATION OF MATERIAL CONSTANTS

In total, the two-layer viscoplasticity model requires nine material constants over the range of temperatures 20˚C, 500˚C, 700˚C and 900˚C. The process of identification of these constants is complex. Consequently, the identification process is carried out in the following series of steps:

Step 1 - Initial estimate of NLKH constants: The material constant *k* for a particular temperature is determined as the mean of the individual *k* values for each strain range, which are readily estimated from the stabilised stress-strain loops. This is still only an initial estimate due to the fact that this step neglects the effect of isotropic hardening. The ratio $\frac{C}{\gamma}$ is determined as the asymptotic value of $\frac{\Delta\sigma}{2}-k$ plotted against $\frac{\Delta\varepsilon_p}{2}$, corresponding to the saturated value of back stress. The coefficients C and γ are the identified by fitting the following equation, which represents the NLKH relationship between cyclic stress and strain to the measured cyclic stress-strain data [5]:

$$\frac{\Delta\sigma}{2}-k=\frac{C}{\gamma}\tanh\left(\gamma\frac{\Delta\varepsilon_p}{2}\right) \tag{14}$$

Figure 6 shows the identification of the coefficients C and γ for the XN40F tool material at 20˚C, 500˚C, 700˚C and 900˚C for the strain rate of 5×10^{-4} s^{-1}. Similarly the material constants are identified for the strain rate of 5×10^{-3} s^{-1}. The identified material constants are summarised in Table 6. Figures 7 and 8 show the comparison of the NLKH material model predictions (using the latter identified constants) with the experimental stabilized loops over the range of temperatures, for the strain-range of 5×10^{-4} s^{-1}. The correlation for the 5×10^{-3} s^{-1} case was of equivalent quality. The NLKH model is seen to work well for 20˚C and 500˚C but not so well for 700˚C and 900˚C, due to the increasing importance of viscoplastic effects above 500˚C.

Step 2 - Initial estimate of isotropic hardening constants: As described in [6], the relationship representing isotropic hardening for the N^{th} cycle is given by:

$$\frac{\sigma_{Max} - \sigma_{Max0}}{\sigma_{Maxs} - \sigma_{Max0}} = 1 - \exp(-2b\Delta\varepsilon_p N) \tag{15}$$

where σ_{Maxs} and σ_{Max0} are the maximum stresses of the stabilized cycle and the first cycle, respectively. This evolution rule represents cyclic hardening effects. Initial estimates of the isotropic hardening constants Q_∞ and b were obtained from the evolving stress-strain loops corresponding to a strain range of 0.6% and the strain rate of 5×10^{-4} s^{-1} at 20, 500 and 700˚C (as shown above negligible isotropic hardening occurs at 900˚C). The material parameter Q_∞ was determined as the difference between σ_{Maxs} and σ_{Max0}. The parameter b is identified by fitting Equation 15 to the measured stress–strain data, as shown in Figure 9. The k (elastic domain) value for the NLKH model determined from the stabilized stress-strain loops is then modified by subtracting Q_∞ from it. The identified kinematic-isotropic material constants are summarised in Table 6. Figure 10 shows the comparison of the combined material model predictions using identified constants at 20˚C, 500˚C and 700˚C.

Step 3 – Identification of creep constants and two-layer constant: The secondary creep constants A and n were identified by plotting experimental data from stress relaxation tests as $Log(\dot{\sigma})$ versus $Log\ \sigma$. Figure 11a shows the comparison of power law creep model and experimental stress relaxation at 700 and 900˚C. The identified power law creep constants for 700 and 900˚C are given in Table 7. The user-specified ratio f from Equation 13 was identified by fitting and comparing the two-layer model with the experimental stress relaxation results, using the latter A and n values. Figure 11b shows the comparison of the two-layer model with the experimental stress relaxation at 700 and 900˚C. The identified f value is also given in Table 7.

VALIDATION OF TWO-LAYER VISCOPLASTIC MODEL

Figures 12 to 14 show comparisons of the two-layer model, using the identified temperature-dependent constants, with the measured test data, for different strain-rates and strain-ranges at 700 and 900˚C. The final, stabilized, isothermal predictions for 20˚C and 500˚C are shown in Figure 7.

Figure 15 shows the predicted and measured effect of strain-rate at 900˚C where the predictions are from the two-layer model; the correlation for lower temperatures was of equivalent quality.

The two layer model was also applied to simulative thermo-mechanical fatigue (TMF) tests, designed to represent the temperature and stress-strain cycling associated with the most damaging phase of the SPF die cycle, based on thermo-mechanical analyses similar to those presented in [7].

Figure 16 shows the typical strain and temperature loading history used for the out-of-phase (OP) TMF tests (see Table 4 for TMF test details). The temperature is cycled between 750˚C and 900˚C with a 120 seconds strain hold in compression at 900˚C, representing the dwell period of the SPF forming cycle. Figure 14 shows the comparison of the resulting stabilized anisothermal stress-strain loop for the same loading conditions and the corresponding FE-predicted response, based on the isothermally-identified material constants from Tables 6 and 7 with the two-layer model. The comparison shows very good correlation with the experimental data. A similar quality of correlation was observed for other TMF tests performed.

CONCLUSIONS

- The isothermal cyclic elastic-plastic characterisation of XN40F under strain range, temperature (from 20^{o}C to 900^{o}C) and strain-rate conditions representative of typical superplastic forming die conditions has been presented.
- The identified isothermal constants for combined non-linear kinematic-isotropic cyclic plasticity have been identified from strain-controlled tests; comparison of the implemented time-independent plasticity constants against the cyclic tests showed reasonable correlation with the largest discrepancies occurring at high temperatures (above 500^{o}C), due presumably to the omission of rate-dependent effects.
- The material constants have been identified for a two-layer viscoplasticity model which combines cyclic plasticity and viscoplasticity from the isothermal cyclic tests and stress relaxation tests for 700^{o}C and 900^{o}C.
- The identified constants with the two-layer viscoplastic model gave excellent correlation with the cyclic stress-strain response of the material across a range of temperatures and successfully captured the effect of strain-rate.
- The ABAQUS aniothermal implementation of the two-layer model was also shown to successfully predict the measured anisothermal cyclic stress-strain response of the material.

ACKNOWLEDGMENTS

The authors wish to thank Ian Leaver and John Chippendale of BAE Systems, Salmesbury for helpful discussions. The first author would also like to thank BAE Systems for funding. Thanks also to Mr Chris Hyde and Mr Tom Buss for research on the optimum coil configuration and TMF testing.

REFERENCES

[1] Gao, C.Y., Lours, P., Bernhart, G., *Thermomechanical stress analysis of superplastic forming tools*, Journal of Materials Processing Technology, 169, 2005, 281-291

[2] Hyde, C.J., Sun, W., Leen, S.B., "Cyclic thermo-mechanical material modelling and testing of 316 stainless steel", *Creep and Fracture in High Temperature Components – Design and Life Assessment*, EMPA, Zurich, Switzerland, 21-23 April, 2009.

[3] Shang, J. *Thermo-mechanical life assessment of superplastic forming tools*, PhD Thesis, University of Nottingham, September 2005.

[4] ABAQUS User and Theory Manuals, Version 6.5, HKS Inc., Rhode Is., US, 2004

[5] Kichenin, J., Dang Van, K., Boytard, K., *Finite element simulation of a new two-dissipative mechanisms model for bulk medium-density polythelene*, J Materials Science, 31, 1996, 1653-1661.

[6] Lemaitre J., Chaboche J., *Mechanics of solid materials*, Cambridge University Press, 1990.

[7] Deshpande, A.A., Leen, S. B. and Hyde, T. H., *Finite element based predictions of life limiting behaviour for a large SPF tool*, Materialwissenschaft und Werkstofftechnik, 39(4-5), 2008, 309-316

Table 1. Composition of the SPF tool material XN40F.

Table 2. Temperature-dependent thermal properties of XN40F material, from [3].

Table 3 Monotonic mechanical properties of XN40F material at different temperatures for strain rate of 8×10^{-4}/s [3].

Table 4. Summary of test programme

Table 6 Combined nonlinear/isotropic hardening parameters for XN40F alloy for a strain rate of 5×10^{-4} s^{-1}

Table 7 Power law creep and two-layer viscoplasticity constants for XN40F alloy

Fig. 1 (a) Geometry of thermo-mechanical fatigue test specimen and (b) photograph of in-situ specimen with induction coil with extensometer.

Fig. 2. Measured stabilised stress-strain loops for XN40F for different temperatures and strain-ranges for a strain rate of 5×10^{-4} s^{-1}.

Fig. 3. Stress-strain loops representing cyclic hardening behaviour of XN40F alloy for 0.6% strain range and strain rate of 5×10^{-4} s^{-1} at 20˚C, 500˚C, 700˚C and 900˚C.

Fig. 4. Stress histories from a stress relaxation tests carried out at 700˚C and 900˚C on XN40F alloy.

Fig. 5. One dimensional rheological representation of the two-layer viscoplasticity model [5].

Fig. 6 Identification of coefficients C and γ for strain rate 5×10^{-4} s^{-1}.

Fig. 7 Comparison of predicted NLKH model responses using identified NLKH constants for different strain-ranges at 20˚C and 500˚C.

Fig. 8. Comparison of predicted NLKH model responses using identified NLKH constants for different strain-ranges at 700˚C and 900˚C.

Fig.9 Identification of isotropic hardening parameter b for XN40F alloy for 5×10^{-4} s^{-1} strain rate and 0.6% strain range at: (a) 20˚C, (b) 500˚C and (c) 700˚C.

Fig. 10. Comparison of combined kinematic-isotropic hardening model with tests at 20˚C, 500˚C and 700˚C.

Fig. 11. Validation of power law creep constants A and n and two-layer viscoplasticity constant f at 700 and 900˚C.

Fig. 12. Validation of identified NLKH and creep two-layer model constants for different strain-ranges at 700˚C for a strain-rate of 5×10^{-4} s^{-1}.

Fig. 13. Validation of identified NLKH and creep two-layer model constants for different strain-ranges at 900˚C for a strain-rate of 5×10^{-3} s^{-1}.

Fig. 14. Validation of identified NLKH and creep two-layer model constants for different strain-ranges at 900˚C for a strain-rate of 5×10^{-4} s^{-1}.

Fig. 15. Measured and predicted (two-layer model) strain-rate effect on cyclic stress-strain curve at 900˚C.

Fig. 16. Typical imposed strain-temperature cycle for simulative TMF test.

Fig. 17. Comparison of FE-predicted and measured stabilised cyclic stress-strain response for simulative TMF test ($\Delta\varepsilon$ = 1 %.).

Table 1. Composition of the SPF tool material XN40F.

Elements	C	Ni	Cr	Fe
Weight %	0.35	40.0	20.0	Balance

Table 2. Temperature-dependent thermal properties of XN40F material, from [3].

Thermal conductivity		Thermal expansion		Specific heat	
Temp [°C]	[W/m/K]	Temp [°C]	x10^{-6}[/˚C]	Temp [°C]	[J/kg/K]
20	11	20-100		0	437
500	20	20-500	15.8	500	536
850	26	20-850	17.35	850	603
950	28	20-950	17.7	950	618

Table 3 Monotonic mechanical properties of XN40F material at different temperatures for strain rate of 8×10^{-4}/s [3].

Temp [°C]	Young's modulus [GPa]	0.2% Yield strength [MPa]	UTS [MPa]	Elongation [%]
20	162	172	332	3
500	130	145	320	6
700	110	110	286	16
900	92	107	120	37

Table 4. Summary of test programme

Test No.	Test type	Temperature	Test Specifications	Material parameters
1	Isothermal multi-strain range fatigue tests	20ºC, 500ºC, 700ºC and 900ºC	R_ε = -1 Triangular waveform $\Delta\varepsilon$ = 0.4% 0.6%, 0.8%,1.2%,1.4% Strain rates: 5×10^{-3} s^{-1}, 5×10^{-4} s^{-1}	Stabilized stress-strain loops; C and γ
2	Isothermal strain controlled fatigue tests	900ºC	R_ε =-1 Triangular waveform $\Delta\varepsilon$ =0.8%, 1.2% Strain rate: 2.5×10^{-4} s^{-1}	IF life based on 15% drop in maximum stress
3	TMF OP strain controlled tests	750 to 900ºC	R_ε = -1 Triangular waveform $\Delta\varepsilon$ = 0.8%, 1.0%, 1.2% Strain rate: 2.5×10^{-4} s^{-1} No hold period	TMF life based on 15% drop in maximum stress
4	TMF OP strain controlled tests with hold period in compression	750 to 900ºC	R_ε = -1 Δε =0.8%, 1.0%, 1.2% Strain rate:2.5×10^{-4} s^{-1} Hold period: 120 sec	TMF life based on 15% drop in maximum stress
5	Strain controlled TMF OP representative SPF tool test	750 to 900ºC	$R_\varepsilon \neq$-1 $\Delta\varepsilon$ =0.3% Strain rate: 1×10^{-4} s^{-1} Hold period: 120 sec in compression	TMF life based on 15% drop in maximum stress
6	Stress relaxation tests	500, 700 and 900ºC	$\Delta\varepsilon$ = 0.15% Hold period: 360 sec	Secondary Creep constants

Table 6 Combined nonlinear/isotropic hardening parameters for XN40F alloy for a strain rate of 5×10^{-4} s^{-1}

Temp, ˚C	k (MPa)	Q_∞ (MPa)	b	C (MPa)	γ
20	125	50	35	82000	656
500	104	50	20	55000	393
700	101	50	24	32000	267
900	60	0	-	8000	320

Table 7 Power law creep and two-layer viscoplasticity constants for XN40F alloy

Temp [˚C]	A [MPa^{-n}s^{-1}]	n	f
700	2.68E-15	4.68	0.92
900	3.48E-14	5.5	0.99

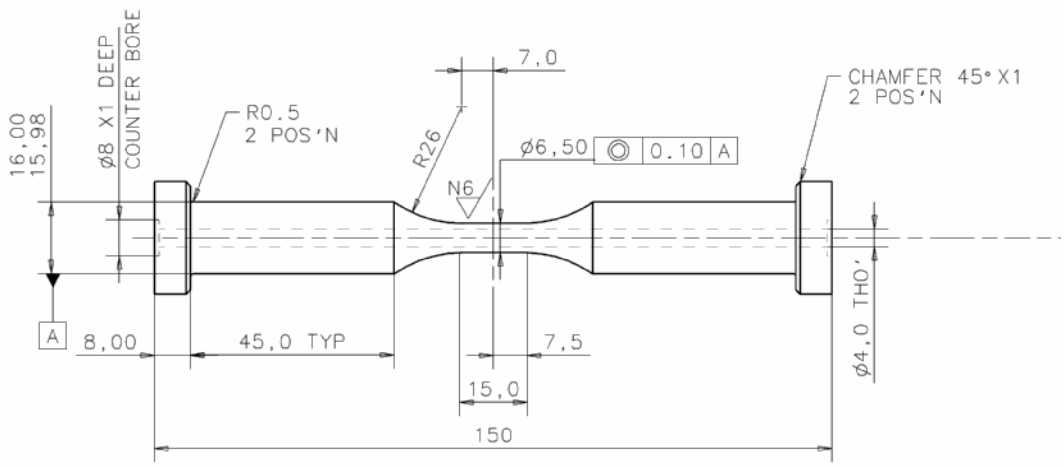

(a)

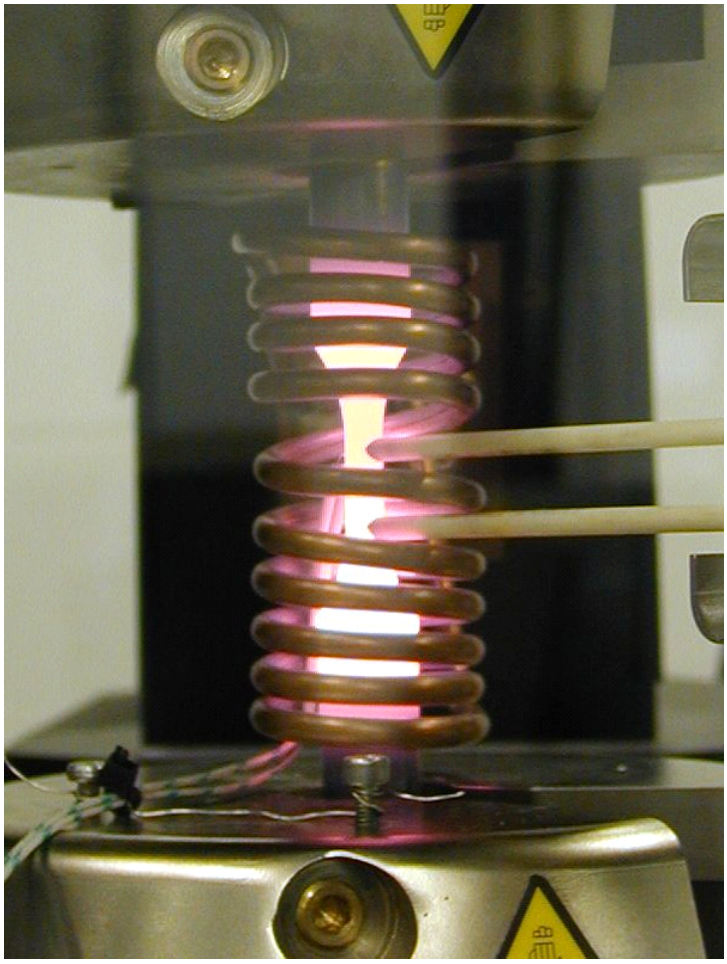

(b)

Fig. 1 (a) Geometry of thermo-mechanical fatigue test specimen and (b) photograph of in-situ specimen with induction coil with extensometer.

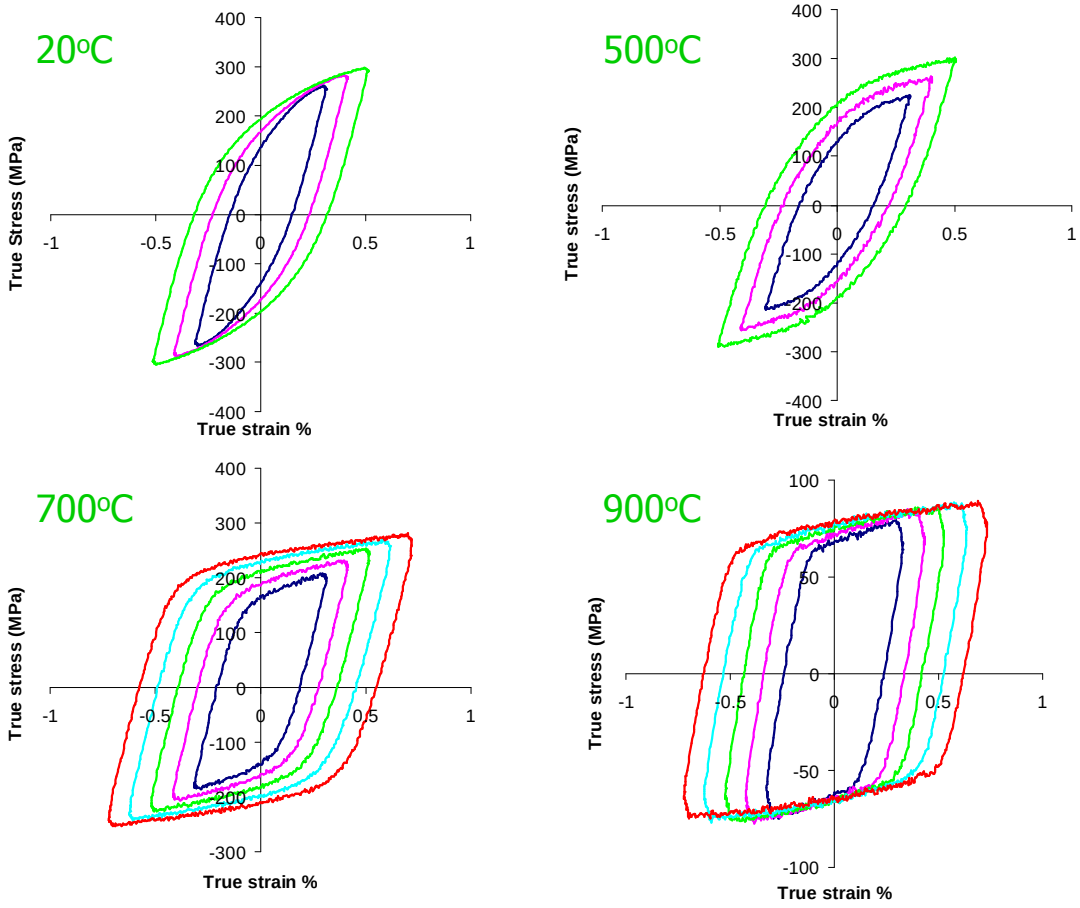

Fig. 2. Measured stabilised stress-strain loops for XN40F for different temperatures and strain-ranges for a strain rate of 5×10^{-4} s^{-1}.

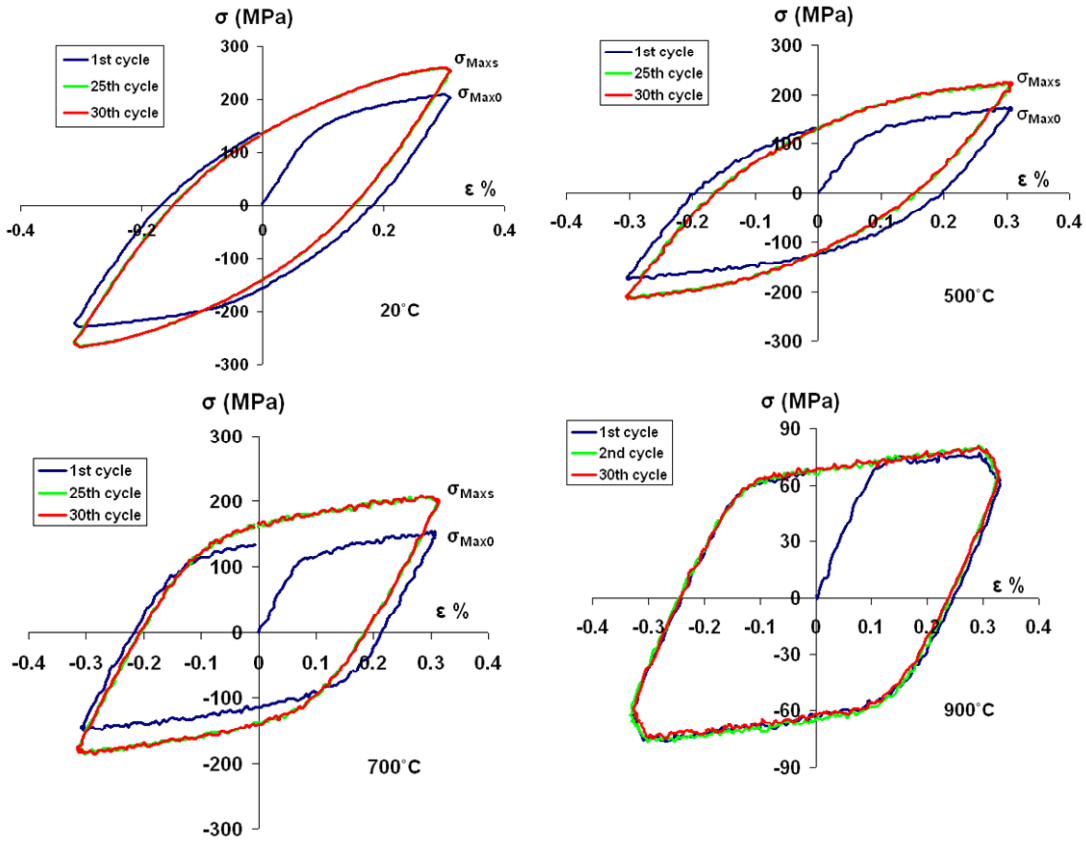

Fig. 3. Stress-strain loops representing cyclic hardening behaviour of XN40F alloy for 0.6% strain range and strain rate of 5×10^{-4} s^{-1} at 20˚C, 500˚C, 700˚C and 900˚C.

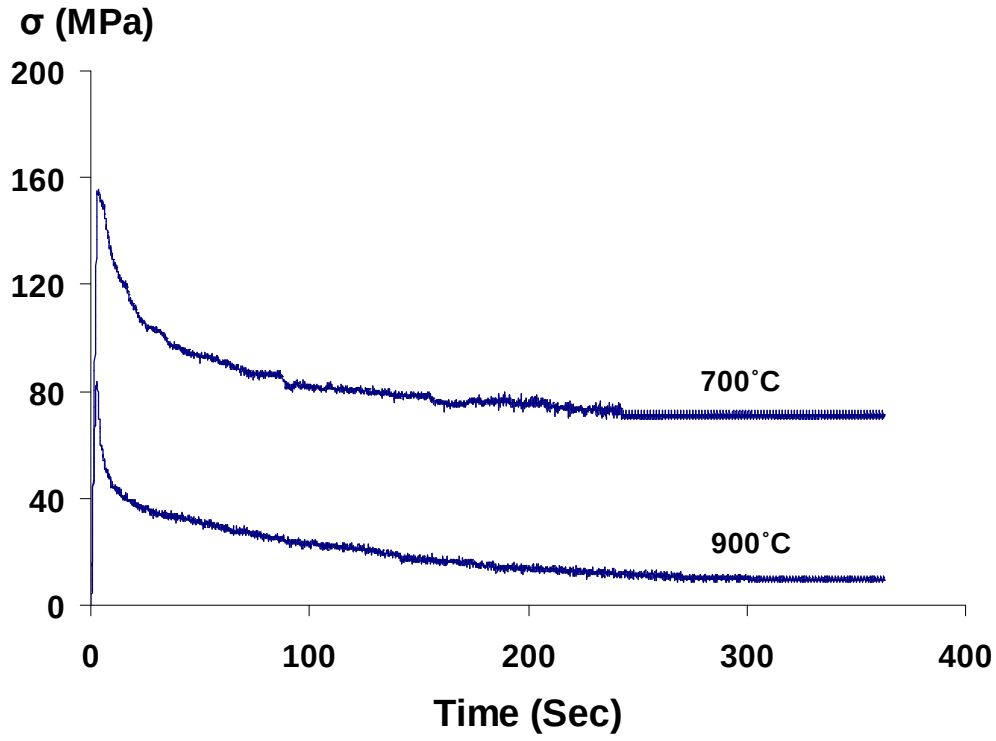

Fig. 4. Stress histories from a stress relaxation tests carried out at 700˚C and 900˚C on XN40F alloy.

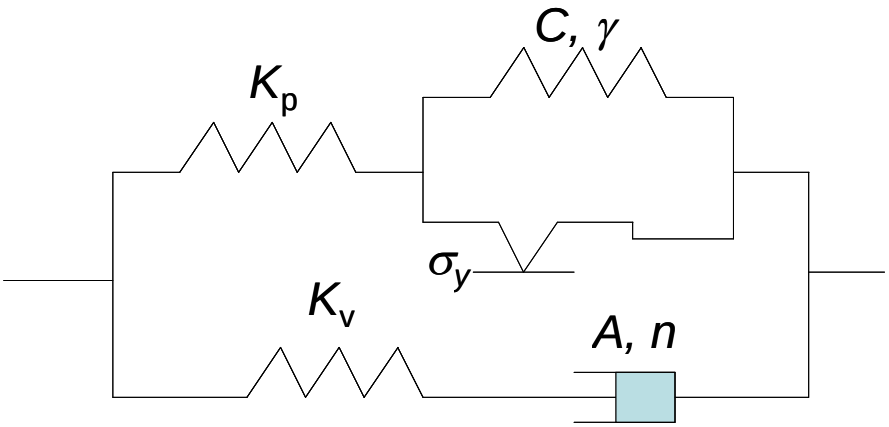

Fig. 5. One dimensional rheological representation of the two-layer viscoplasticity model [5].

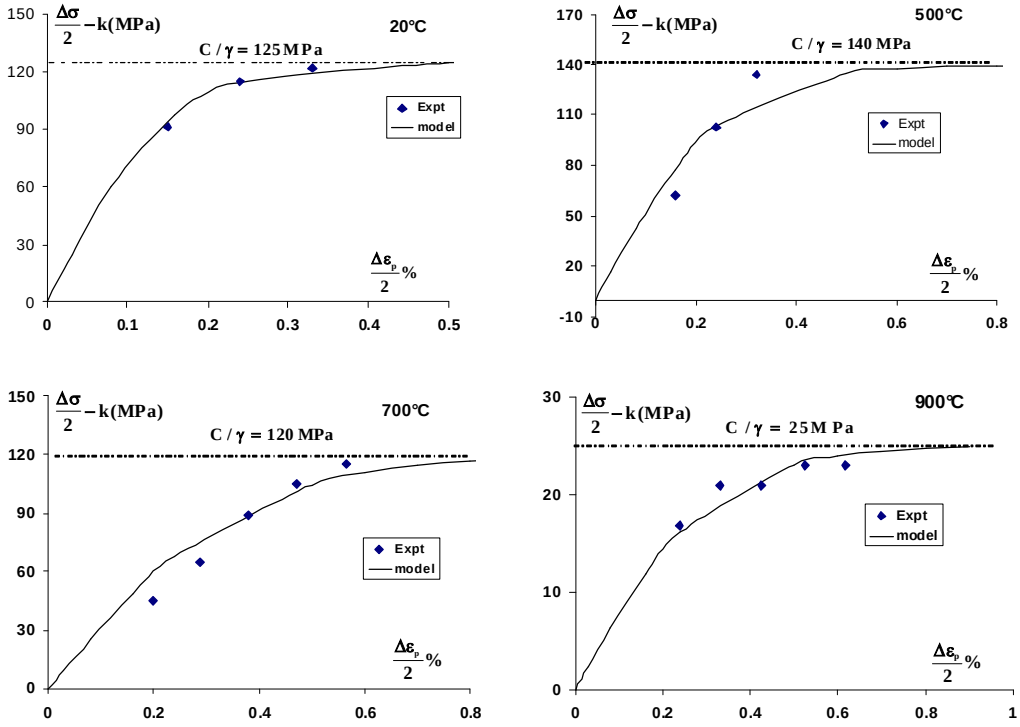

Fig. 6 Identification of coefficients *C* and γ for strain rate 5×10^{-4} s^{-1}.

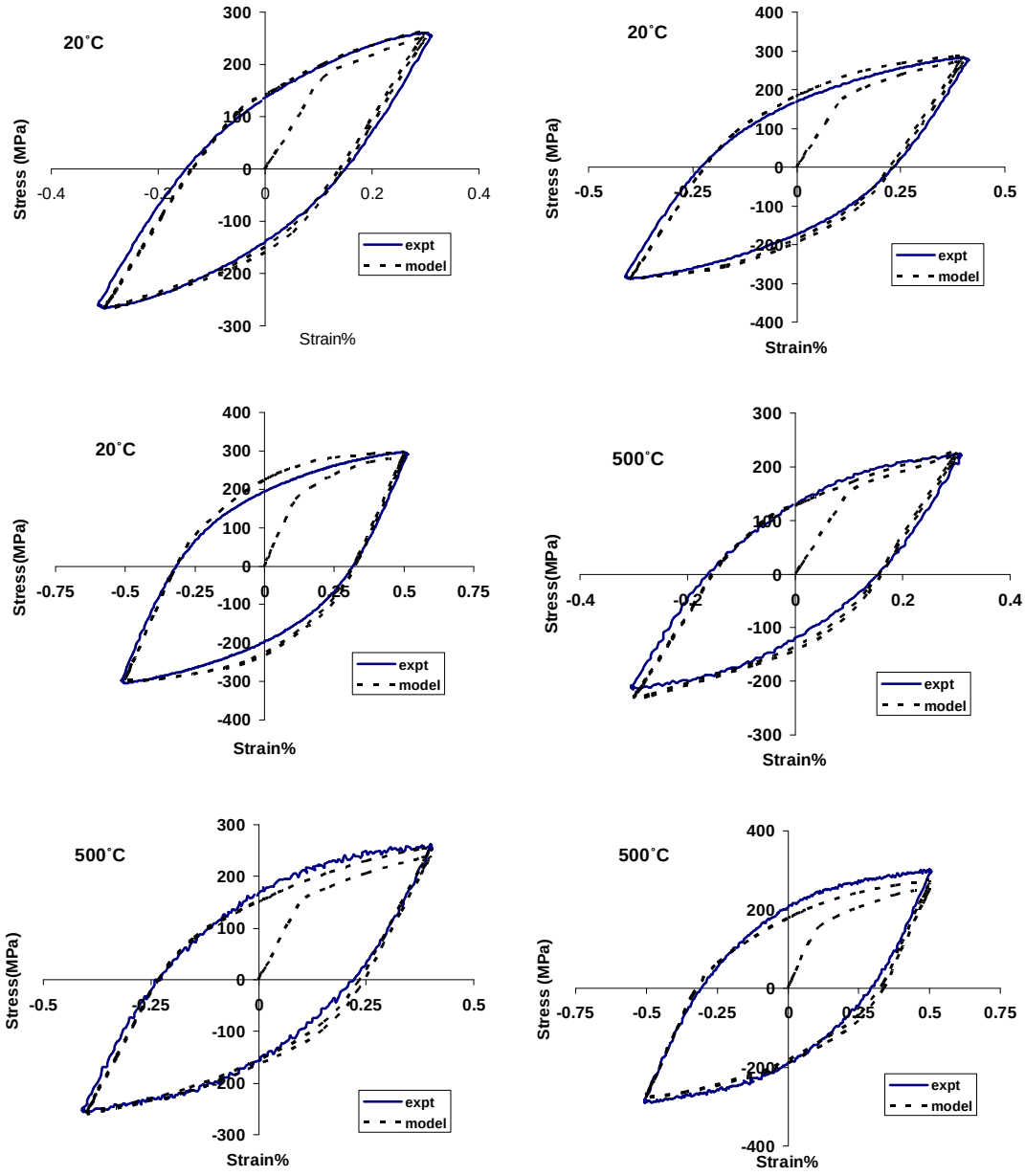

Fig. 7 Comparison of predicted NLKH model responses using identified NLKH constants for different strain-ranges at 20˚C and 500˚C.

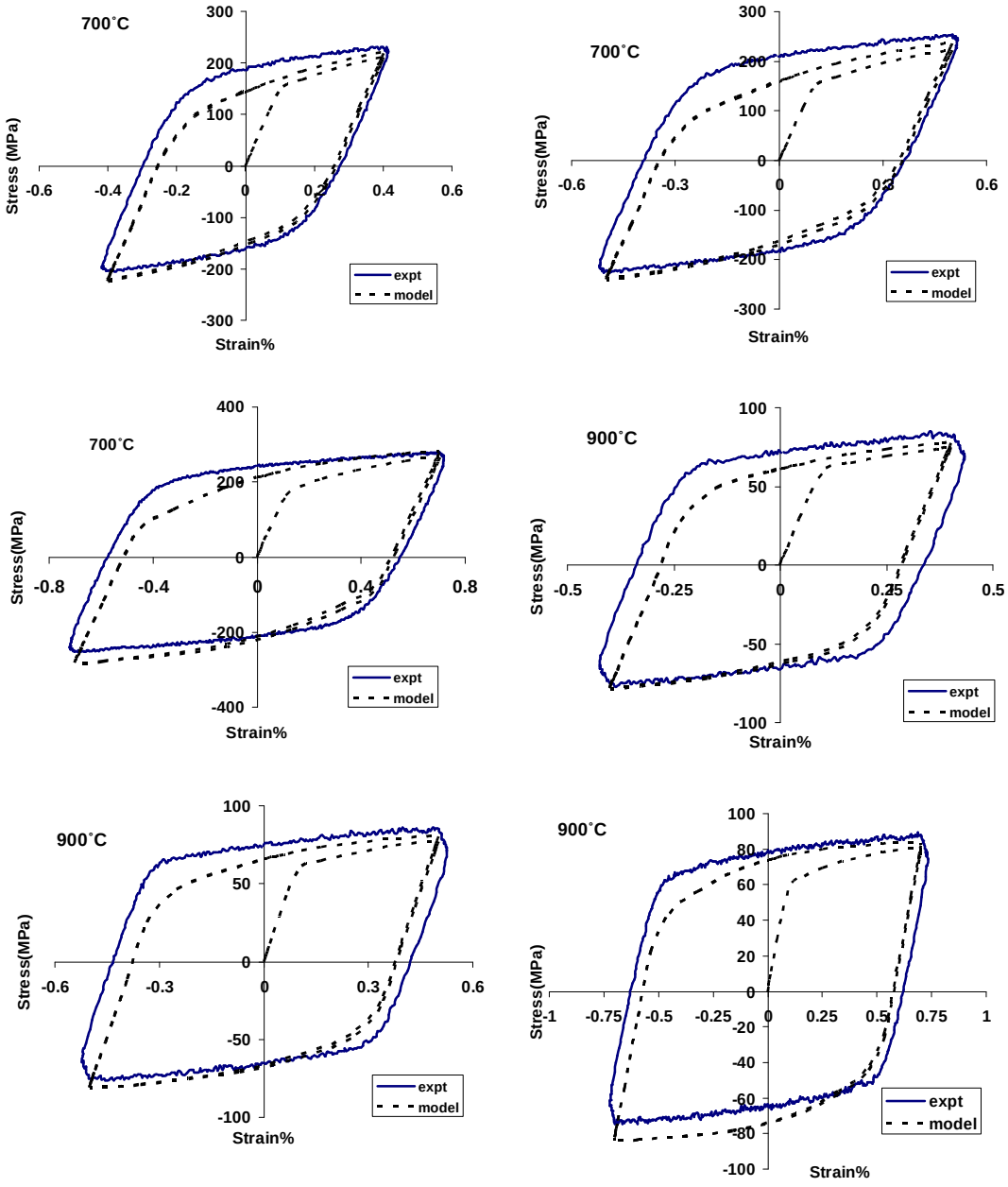

Fig. 8. Comparison of predicted NLKH model responses using identified NLKH constants for different strain-ranges at 700˚C and 900˚C.

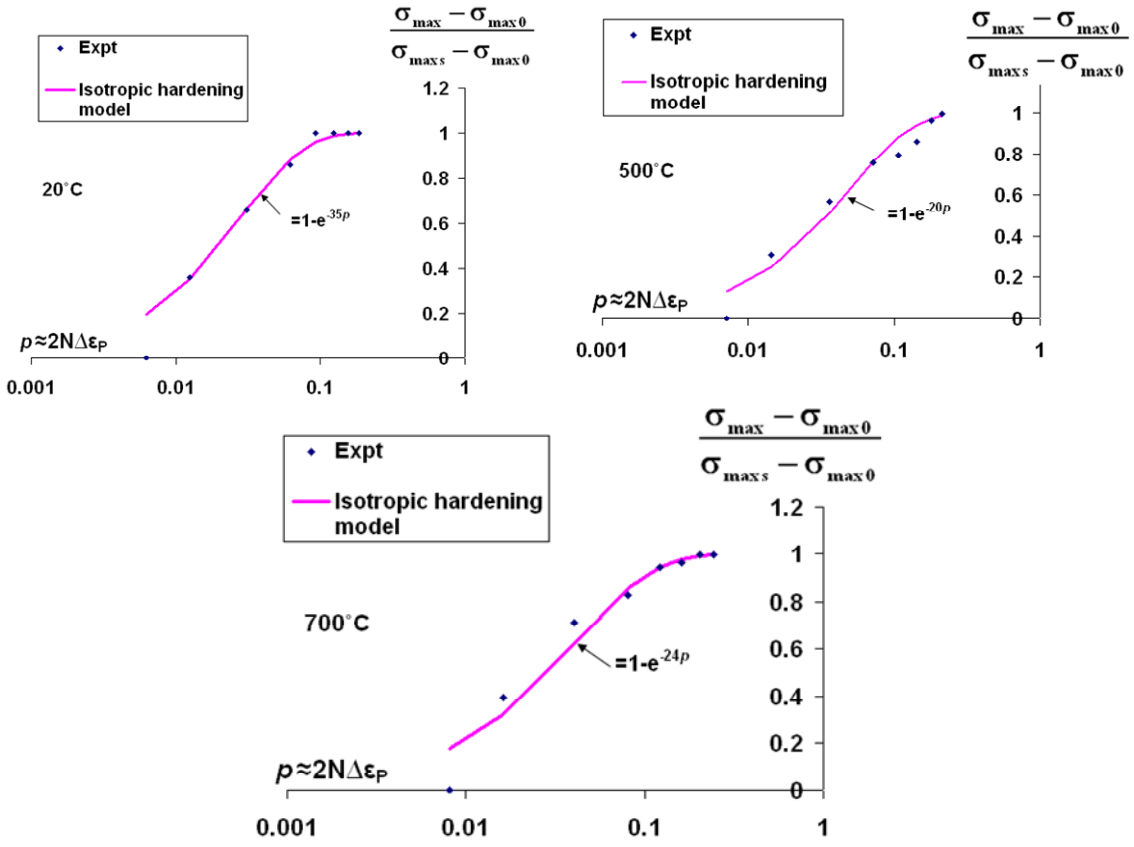

Fig.9 Identification of isotropic hardening parameter *b* for XN40F alloy for 5×10^{-4} s^{-1} strain rate and 0.6% strain range at: (a) 20˚C, (b) 500˚C and (c) 700˚C.

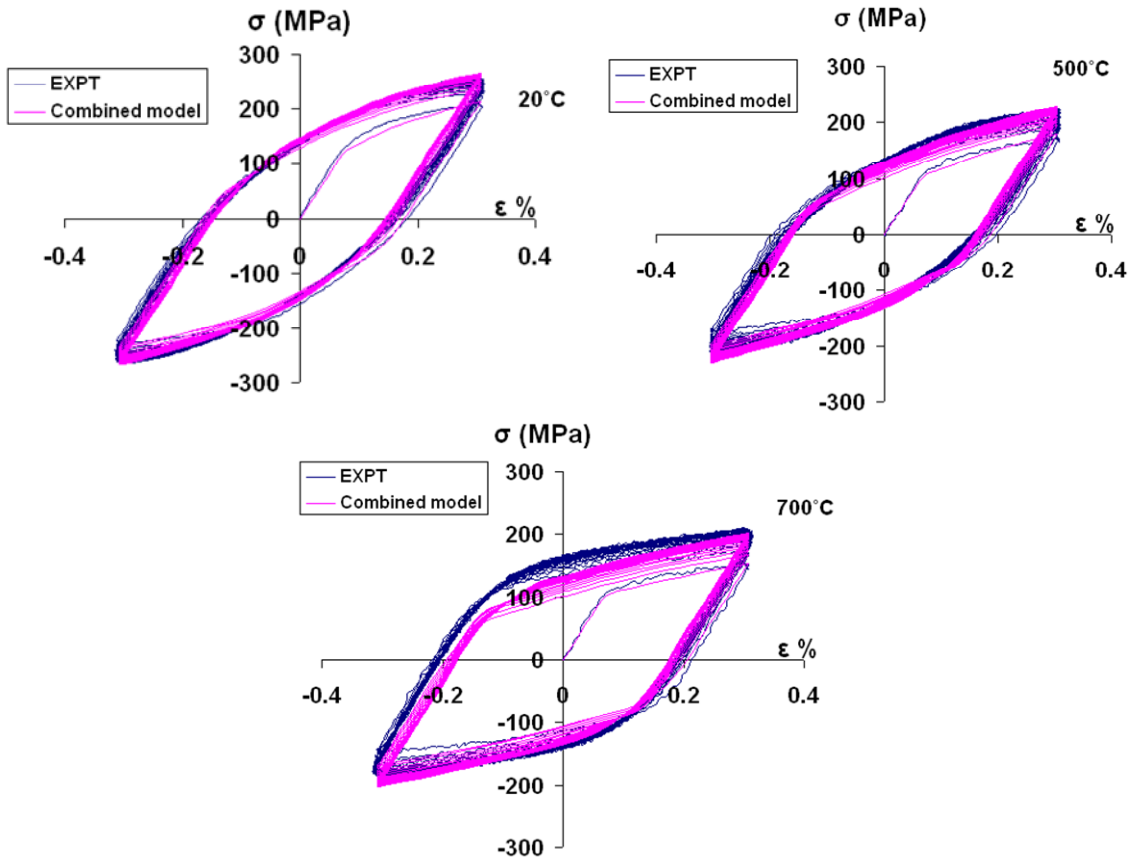

Fig. 10. Comparison of combined kinematic-isotropic hardening model with tests at 20˚C, 500˚C and 700˚C.

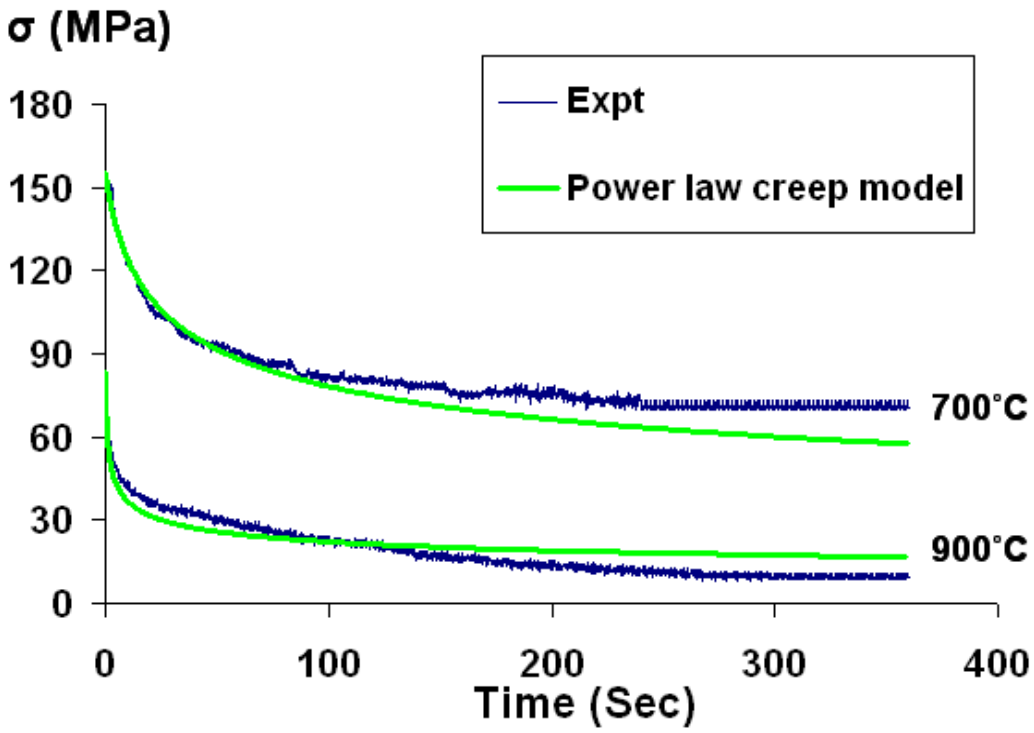

(a)

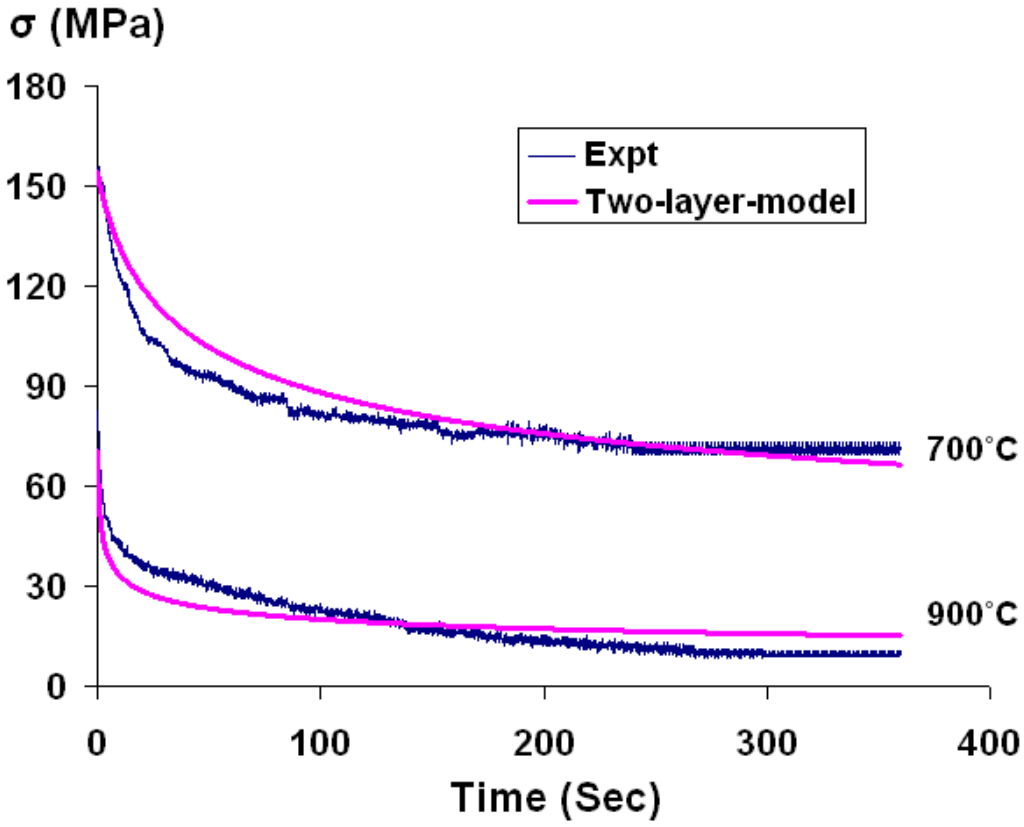

(b)

Fig. 11. Validation of power law creep constants *A* and *n* and two-layer viscoplasticity constant *f* at 700 and 900˚C.

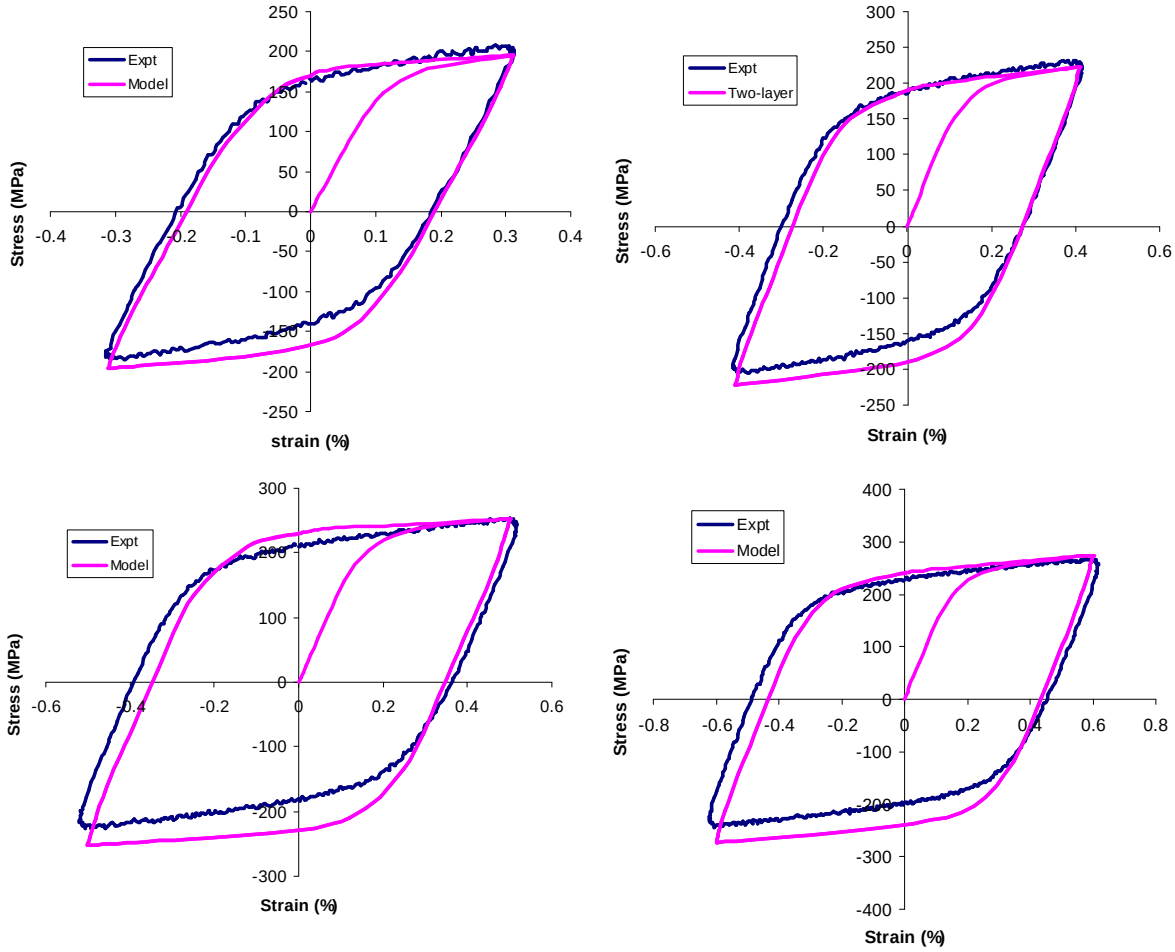

Fig. 12. Validation of identified NLKH and creep two-layer model constants for different strain-ranges at 700˚C for a strain-rate of 5×10^{-4} s^{-1}.

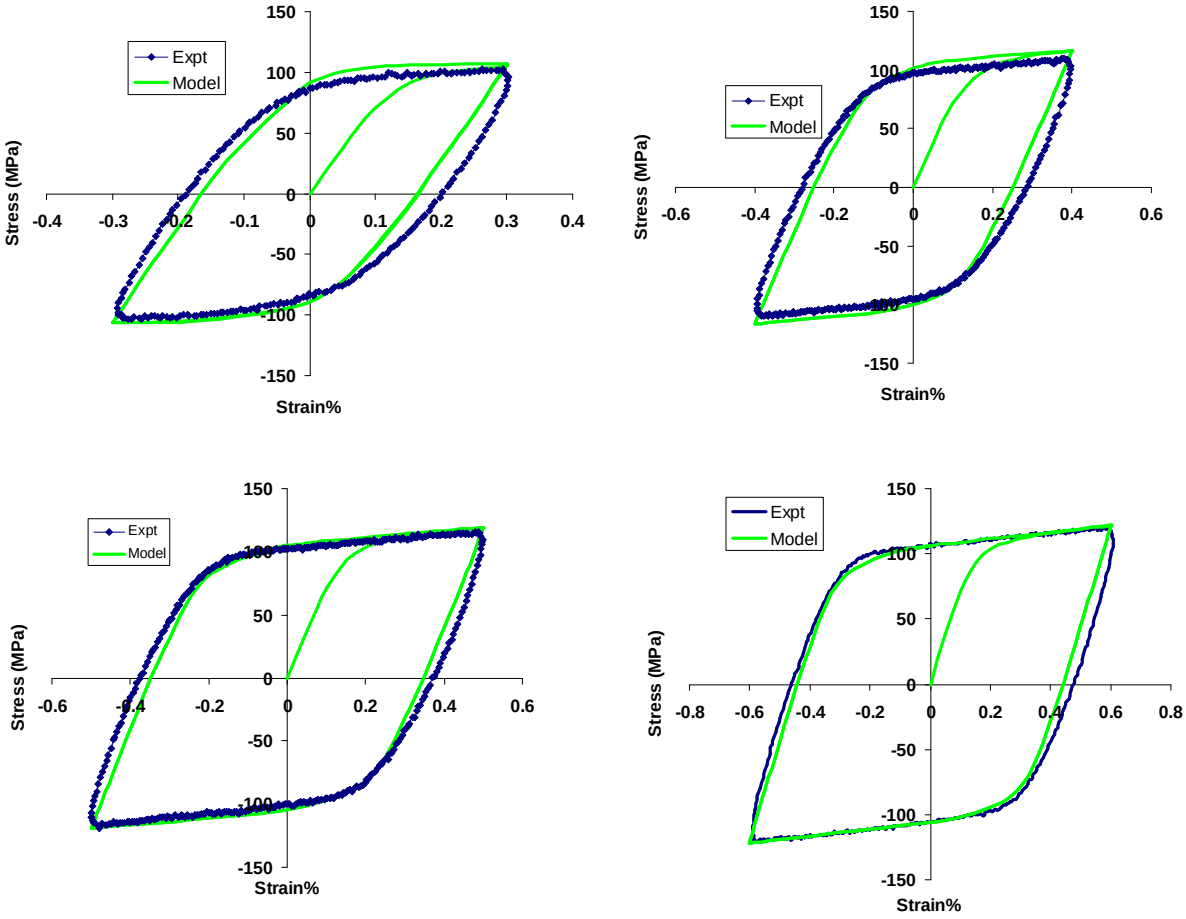

Fig. 13. Validation of identified NLKH and creep two-layer model constants for different strain-ranges at 900˚C for a strain-rate of 5×10^{-3} s^{-1}.

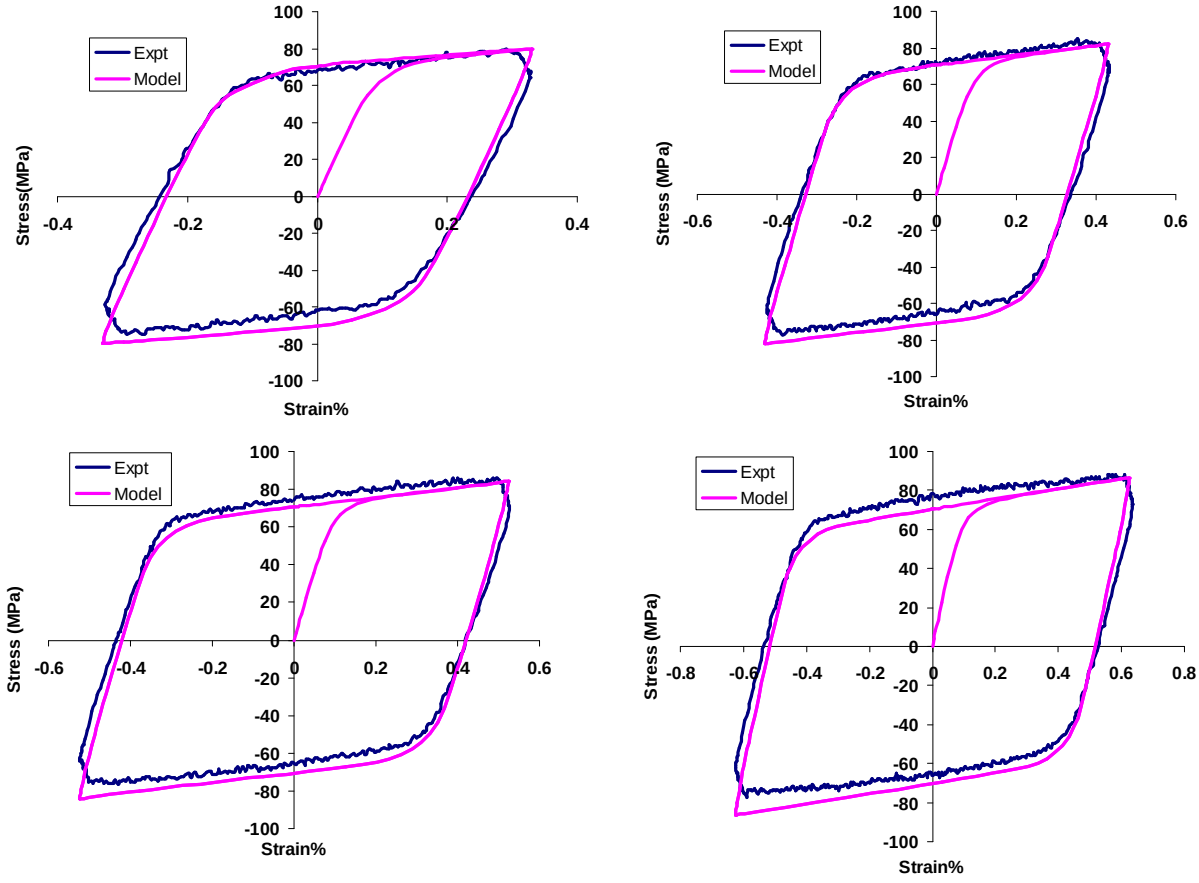

Fig. 14. Validation of identified NLKH and creep two-layer model constants for different strain-ranges at 900˚C for a strain-rate of 5×10^{-4} s^{-1}.

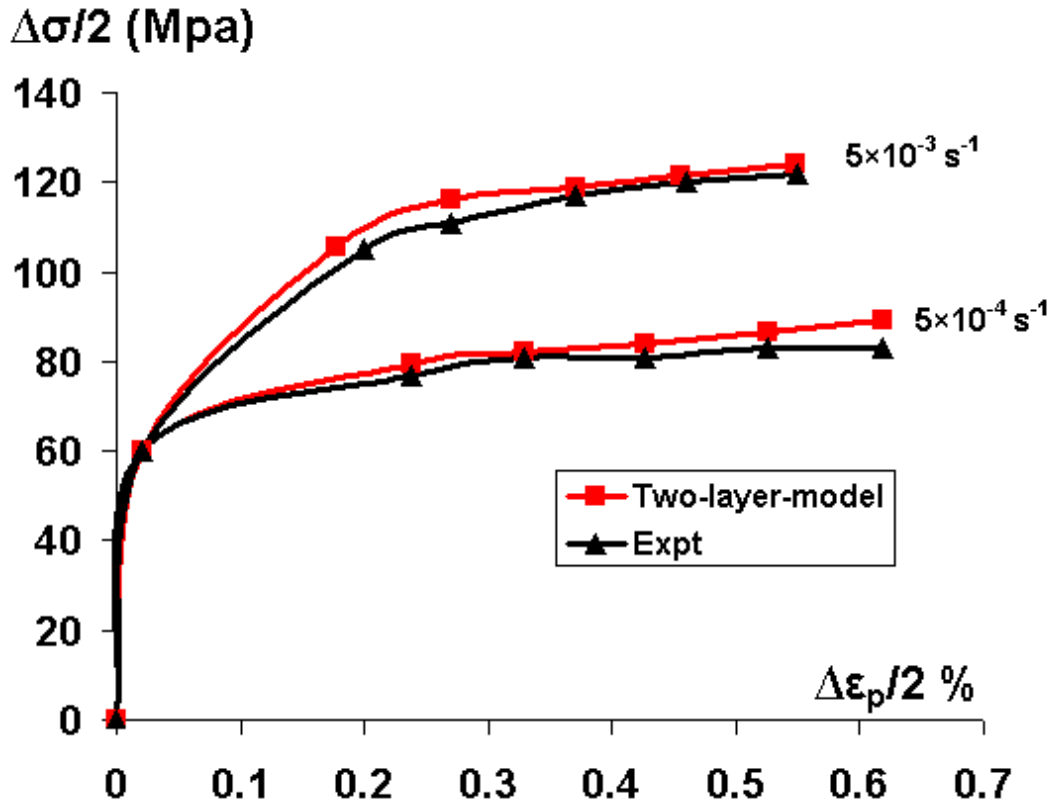

Fig. 15. Measured and predicted (two-layer model) strain-rate effect on cyclic stress-strain curve at 900˚C.

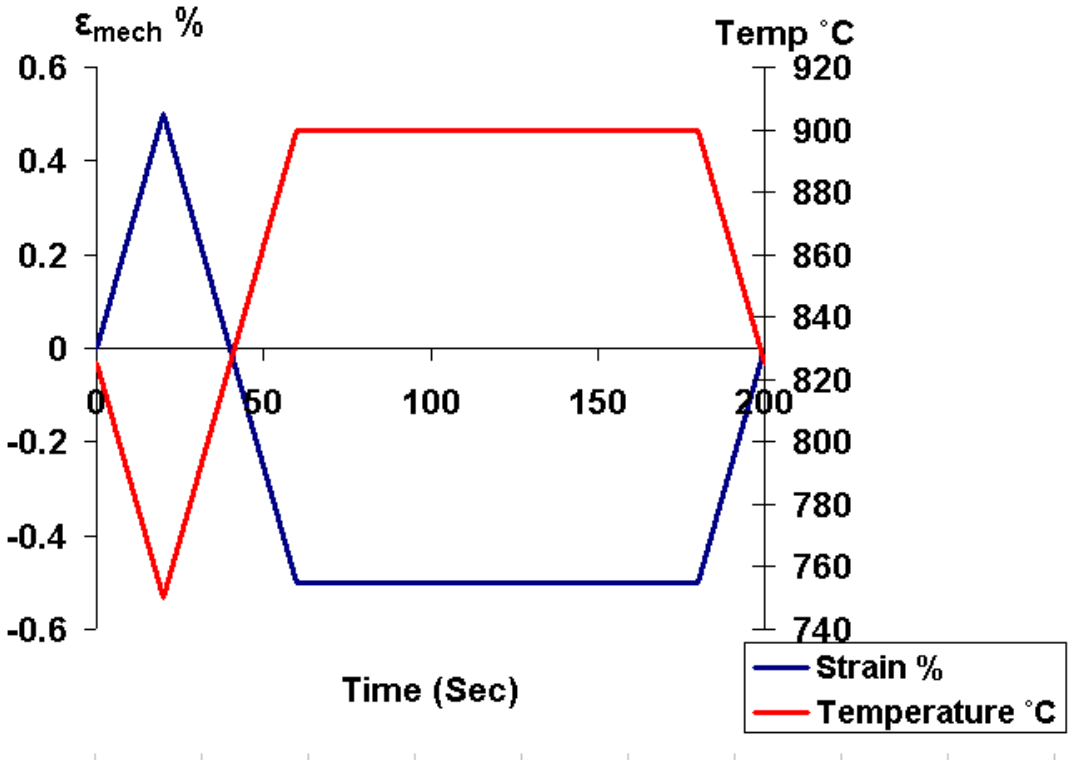

Fig. 16. Typical imposed strain-temperature cycle for simulative TMF test.

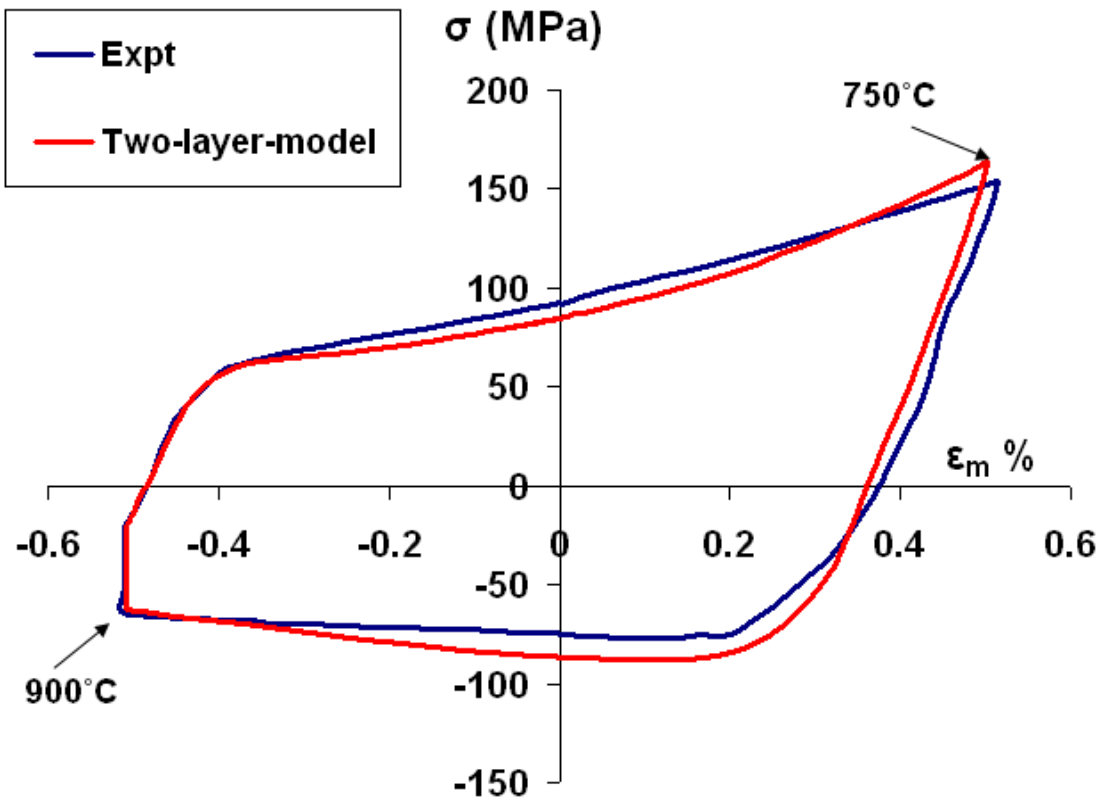

Fig. 17. Comparison of FE-predicted and measured stabilised cyclic stress-strain response for simulative TMF test ($\Delta\varepsilon$ = 1 %.).